

## Heterogeneity of Radial Glia-Like Cells in the Adult Hippocampus

ELIAS GEBARA,<sup>a</sup> MICHAEL ANTHONY BONAGUIDI,<sup>b</sup> RUTH BECKERVORDER SANDFORTH,<sup>c</sup>  
SÉBASTIEN SULTAN,<sup>a</sup> FLORIAN UDRY,<sup>a</sup> PIETER-JAN GIJS,<sup>a</sup> DIETER CHICHUNG LIE,<sup>c</sup> GUO-LI MING,<sup>b,d,e</sup>  
HONGJUN SONG,<sup>b,d,e</sup> NICOLAS TONI<sup>a</sup>

**Key Words.** Adult stem cells • Nervous system • Neural stem cell • Somatic stem cells • Stem cell-microenvironment interactions

<sup>a</sup>Department of Fundamental Neuroscience, University of Lausanne, rue du Bugnon, Lausanne, Switzerland;

<sup>b</sup>Institute for Cell Engineering, <sup>d</sup>Department of Neurology, <sup>e</sup>The Solomon Snyder Department of Neuroscience, Johns Hopkins University School of Medicine, Baltimore, Maryland, USA; <sup>c</sup>Institute of Biochemistry, Friedrich-Alexander Universität, Erlangen-Nürnberg, Fahrstrasse, Erlangen, Germany

Correspondence: Nicolas Toni, Ph.D., 9, rue du Bugnon, 1005 Lausanne, Switzerland.  
Telephone: 4121-692-5133;  
Fax: 4121-692-5105;  
e-mail: Nicolas.toni@unil.ch

Received July 3, 2015; accepted for publication November 8, 2015; first published online in STEM CELLS EXPRESS January 4, 2016.

© AlphaMed Press  
1066-5099/2016/\$30.00/0

<http://dx.doi.org/10.1002/stem.2266>

### ABSTRACT

Adult neurogenesis is tightly regulated by the neurogenic niche. Cellular contacts between niche cells and neural stem cells are hypothesized to regulate stem cell proliferation or lineage choice. However, the structure of adult neural stem cells and the contact they form with niche cells are poorly described. Here, we characterized the morphology of radial glia-like (RGL) cells, their molecular identity, proliferative activity, and fate determination in the adult mouse hippocampus. We found the coexistence of two morphotypes of cells with prototypical morphological characteristics of RGL stem cells: Type  $\alpha$  cells, which represented 76% of all RGL cells, displayed a long primary process modestly branching into the molecular layer and type  $\beta$  cells, which represented 24% of all RGL cells, with a shorter radial process highly branching into the outer granule cell layer-inner molecular layer border. Stem cell markers were expressed in type  $\alpha$  cells and coexpressed with astrocytic markers in type  $\beta$  cells. Consistently, *in vivo* lineage tracing indicated that type  $\alpha$  cells can give rise to neurons, astrocytes, and type  $\beta$  cells, whereas type  $\beta$  cells do not proliferate. Our results reveal that the adult subgranular zone of the dentate gyrus harbors two functionally different RGL cells, which can be distinguished by simple morphological criteria, supporting a morphofunctional role of their thin cellular processes. Type  $\beta$  cells may represent an intermediate state in the transformation of type  $\alpha$ , RGL stem cells, into astrocytes. STEM CELLS 2016;34:997–1010

### SIGNIFICANCE STATEMENT

Adult neurogenesis results in the formation of new neurons that play a role in learning and memory. The morphology of adult neural stem cells (ANSC) residing in the hippocampus is still poorly-described. The assessment of ANSC is usually performed using morphological criteria. Here, we discovered that ANSC are intermingled with cells of similar morphology but devoid of proliferative properties. These cells display hallmarks of immature astrocytes and are generated by ANSC, suggesting that they represent intermediates in the ANSC-astrocyte transition. Our results are relevant to the process of adult neurogenesis and will refine the assessment of ANSC status *in vivo*.

### INTRODUCTION

The adult mammalian brain retains neural stem cells in two discrete areas, the subventricular zone and dentate gyrus of the hippocampus [1, 2]. Increasing evidence suggests that upon maturation, new neurons are involved in mechanisms of learning and indeed, the stimulation of adult hippocampal neurogenesis increases learning and memory performances [3, 4]. Thus, mechanisms involved in the regulation of adult neurogenesis are of great interest for our understanding of learning and memory and for the potential treatment of memory impairment.

In the hippocampus, adult neural stem cells reside in the subgranular zone (SGZ) of the dentate gyrus and may display a radial glia-like (RGL) morphology. They are characterized by a long process that extends through the granule cell layer (GCL) and widely branches in the outer GCL and in the inner third of the molecular layer [5–8]. Adult neural stem cells in the SGZ may also display shorter, horizontal processes [9, 10] greater proliferative activity than RGL stem cells [11], suggesting the existence of a morphofunctional component in the regulation of quiescence.

During embryonic development, time-lapse imaging showed that RGL stem cells generate neurons which use their parent cell's radial process to migrate to the cortical plate, a mechanism that may underlie the radial organization of the neocortex [12]. In adult neurogenesis, however, the function of the radial process in RGL stem cells is not clearly defined. Although the primary process is often seen alongside dendrites from nascent neurons [13], it is unclear whether it is used for the migration of the newborn neurons or for establishing contacts with the neurogenic niche. Furthermore, clonal analysis suggested that newly formed neurons in the adult hippocampus migrate away from their parent cells [14] and may use the vasculature for a tangential migration [15]. Thus, a potential function of the radial processes of adult RGL stem cells may rather be found in regulating their proliferation or fate through interactions with the local niche [16].

The direct cellular environment of neural stem cells plays a fundamental role in the regulation of adult neurogenesis. Indeed, although proliferating cells reside in the entire central nervous system, adult neurogenesis is restricted to the hippocampus and the subventricular zone. However, when transplanted in the hippocampus, progenitor cells from a non-neurogenic area such as the spinal cord regain the ability to generate neurons and inversely, when transplanted in a non-neurogenic area, hippocampal neural stem cells lose their ability to differentiate into neurons [17]. This indicates that the intrinsic neurogenic potential of central nervous system progenitor cells is controlled by the neurogenic niche.

Several cell types of the neurogenic niche have been shown to play a role in the regulation of the neural stem cell proliferation, including endothelial cells [18], astrocytes [19, 20], neurons [21], or microglia [22, 23]. The effect of niche cells on stem cells may be mediated by the release of soluble molecules such as Wnt3a [19] or GABA [21] or by direct contact such as with microglia [23] or astrocytes [24]. These observations suggest that the complex morphology of RGL stem cells enables the establishment of numerous contacts with a variety of cell types of the hilus, GCL, and molecular layer of the dentate gyrus, all of which may participate to its regulation.

The morphology of the RGL stem cells is still poorly described and in particular, it is still unknown whether there is a structure–function relationship among the population of this highly morphologically variable population of cells. The goal of this study is to examine the fine structure of RGL stem cells in the adult hippocampal niche and to test the possibility that the morphological characteristics of RGL stem cells may reflect their function.

## MATERIALS AND METHODS

### Ethics Statement

This study was carried out in strict accordance with the recommendations in the Guidance for the Care and Use of Laboratory Animals of the National Institutes of Health. All experimental protocols were approved by the Swiss animal experimentation authorities (Service de la consommation et des affaires vétérinaires, Chemin des Boveresses 155, 1066 Epalinges, Switzerland). Every effort was made to minimize the number of animals used and their suffering.

### Experimental Animals

Animals used for this study were adult male mice. *GFAP*-green fluorescent protein (GFP) mice were a kind gift from the laboratory of Helmut Kettenmann (Max-Delbrück center, Berlin, Germany) [25]. They express the GFP under the control of the human glial fibrillary acidic protein (GFAP) promoter. *Nestin*-GFP mice were a kind gift from the laboratory of K. Mori (PRESTO, Kyoto, Japan) [26]. These mice express the GFP under the stem cell-specific promoter *Nestin*. *Nestin::CreER<sup>T2</sup>* and *Z/EG<sup>f/+</sup>* mice were purchased from The Jackson Laboratory (Maine, Bar Harbor, ME, USA, www.jax.org). The *Rosa26tdTomato* reporter mice [27] were a kind gift from the laboratory of Jean-Yves Chatton (Department of Fundamental Neurosciences, University of Lausanne, Switzerland). The *GFAP::CreER<sup>T2</sup>-Rosa YFP* were a kind gift from the laboratory of Andrea Volterra (Department of Fundamental Neurosciences, University of Lausanne, Switzerland).

For clonal analysis, we used the *GFAP::CreER<sup>T2</sup>* and the *Nestin::CreER<sup>T2</sup>* mice. The *Nestin::CreER<sup>T2</sup>* mice were crossed with fluorescent reporter mice *Rosa-tdTomato* or *Z/EG<sup>f/+</sup>*. Tamoxifen (62 mg/ml; Sigma-Aldrich, Buchs, Switzerland www.sigmaaldrich.com; T5648) was prepared in a 5:1 ratio of corn oil to ethanol at 37°C with occasional vortexing. A single tamoxifen or vehicle dose was injected into 8–10 weeks old mice (62 mg/kg intraperitoneally [i.p.]) for *Nestin::CreER<sup>T2</sup>-Z/EG<sup>f/+</sup>* mice, 60 mg/kg for *Nestin::CreER<sup>T2</sup>-Rosa26tdtomato* mice, or 86 mg/kg for the *GFAP::CreER<sup>T2</sup>-RosaYFP* mice.

For exercise and aging experiments, young adult mice were 6-week-old and aged mice were 7.5-month-old at the beginning of the experiment. Runner mice were housed for 2 weeks in standard cages with free access to a running wheel (Fast-Trac; Bio-Serv). Non-runner mice were housed in similar, adjacent cages without running wheel. All mice were housed in a 12-hour light/dark cycle and controlled temperature of 22°C. Food and water were available ad libitum.

### BrdU and D-Serine Administration

All mice were injected i.p. with the thymidine analog bromodeoxyuridine (BrdU, Sigma-Aldrich, Buchs, Switzerland, www.sigmaaldrich.com), at doses of 100 mg/kg in saline. D-Serine was prepared fresh every day and diluted in water containing 0.9% NaCl. Seven-week-old mice were injected i.p. every day with 50 mg/kg of D-serine (Sigma-Aldrich, Buchs, Switzerland, www.sigmaaldrich.com) for 8 consecutive days or with the same volume of vehicle (0.9% NaCl in water).

### Tissue Collection and Preparation

At the end of the experiment, mice received a lethal dose of pentobarbital (10 ml/kg, Sigma-Aldrich, Buchs, Switzerland, www.sigmaaldrich.com) and were perfusion-fixed with 50 ml of 0.9% saline followed by 100 ml of 4% paraformaldehyde (Sigma-Aldrich, Switzerland, www.sigmaaldrich.com) dissolved in phosphate buffer saline (PBS 0.1M, pH 7.4). Brains were then collected, postfixed overnight at 4°C, cryoprotected 24 hours in 30% sucrose, and rapidly frozen. Coronal frozen sections of a thickness of 40 µm (50 µm for clonal analysis) were cut with a microtome-cryostat (Leica MC 3050S) and slices were kept in cryoprotectant (30% ethylene glycol and 25% glycerin in 1X PBS) at –20°C until processed for immunostaining.

## Immunohistochemistry

Immunohistochemistry was performed on 1-in-6 series of section. Sections were washed three times in PBS 0.1 M. BrdU detection required a DNA denaturation for 20 minutes in 2 M HCl at 37°C and rinsed in 0.1 M borate buffer pH 8.5 for 15 minutes. Then, slices were incubated in blocking solution containing 0.3% Triton-X100 and 15% normal serum (normal goat serum (Gibco) or normal donkey serum (Sigma Aldrich, Buchs, Switzerland, www.sigmaaldrich.com depending on the secondary antibody) in PBS 0.1 M. Slices were then incubated 40 hours at 4°C with the following primary antibodies: Chicken anti-GFP (1:500, AnaSpec Inc, Liege, Belgium, www.anaspec.com), Rabbit anti-GFP (1:500, AnaSpec Inc, Liege, Belgium, www.anaspec.com), mouse monoclonal anti-BrdU (1:250, Chemicon International, Schaffhausen, Switzerland, www.merckmillipore.com), rabbit anti-K-i67 (1:200, Abcam, Cambridge, UK, www.abcam.com), rabbit anti-Sox1 (1:500, Abcam, Cambridge, UK, www.abcam.com), rabbit anti-GFAP (1:500, Invitrogen), goat anti-Iba1 (1:200, Abcam, Cambridge, UK, www.abcam.com), rabbit anti-Sox2 (1:500, Millipore, Schaffhausen, Switzerland, www.merckmillipore.com), rabbit anti-NG2 (1:400, Chemicon, Schaffhausen, Switzerland, www.merckmillipore.com) mouse anti-CD133 (Prominin 1, 1:500, Millipore, Schaffhausen, Switzerland, www.merckmillipore.com), mouse anti-Nestin (1:200, Millipore, Schaffhausen, Switzerland, www.merckmillipore.com), rabbit anti-S100B (1:500, Abcam, Cambridge, UK, www.abcam.com), rabbit anti-GLT1 (1:500, Abcam, Cambridge, UK, www.abcam.com). The sections were then incubated for 2 hours in either of the following secondary antibodies: Dylight 488 goat anti-chicken (1:500, Jackson ImmunoResearch, Newmarket, UK, www.jieurope.com), goat anti-rabbit Alexa-488 (1:250, Invitrogen, Zug, Switzerland, www.thermofischer.com) goat anti-mouse Alexa-594 (1:250, Invitrogen, Zug, Switzerland, www.thermofischer.com), goat anti-rabbit Alexa-594 (1:250, Invitrogen, Zug, Switzerland, www.thermofischer.com), donkey anti-goat Alexa-555 (1:250, Invitrogen, Zug, Switzerland, www.thermofischer.com), and donkey anti-rabbit Alexa 647 (1:250, Invitrogen, Zug, Switzerland, www.thermofischer.com). Blood vessels were labeled by Sulforhodamine 101 (Invitrogen, Zug, Switzerland, www.thermofischer.com). 4,6-Diamidino-2-phenylindole (DAPI) was used to reveal nuclei.

## Image Analysis

Images were collected with a Zeiss confocal microscope (Zeiss LSM 710 Quasar Carl Zeiss, Oberkochen, Germany, www.zeiss.com) and cell counts were performed using stereology principles, as described previously [28]. Briefly, for each animal, a 1-in-6 series of section between  $-1.3$  to  $-2.9$  mm from the Bregma was stained with the nucleus marker DAPI and used to measure the volume of the GCL. The granule cell area was traced using Axiovision (Zeiss, Oberkochen, Germany, www.zeiss.com) software and the granule cell reference volume was determined by multiplying the area of the GCL by the distance between the sections sampled (240  $\mu$ m). All cells were counted in the entire thickness of the sections in a 1-in-6 series of section (240  $\mu$ m apart) with a 40 $\times$  objective. All cells were counted blind with regard to the mouse status. The number of immunolabeled cells was then related to GCL sectional volume and multiplied by the reference volume to estimate the total number of immunolabeled cells. RGL cells were counted in the SGZ of the dentate gyrus.

Clones were analyzed as described in Bonaguidi et al. [14]. Briefly, the tamoxifen dose was calibrated for each mouse line, so as to obtain a maximum of four clones per hippocampus. Clonal relation was then assessed within a distance of 150  $\mu$ m from the type  $\alpha$  RGL cell. Since progenies do not migrate more than 125  $\mu$ m from the mother cell (as observed 2 months after tamoxifen injection in Bonaguidi et al. [14], Fig. 1F), this distance is sufficient to guarantee more than 90% probability as a clone.

## Statistical Analysis

Hypothesis testing was two-tailed. All analyses were performed using JMP10 software. First, Shapiro-Wilk tests were performed on each group of data to test for distribution normality. For normal distribution we performed parametric tests. When the distribution was not normal, a nonparametric Kruskal-Wallis test was used. Homoscedasticity of variances was tested by Bartlett's test and adequate analysis of variance was performed, followed by a post hoc multiple comparisons procedure *t* test with Bonferroni correction. For two sample comparisons, when the distribution was normal, the equality of variances of the groups was tested by a bilateral F-test and the adequate unpaired *t* test was used. All data are presented as mean  $\pm$  SEM.

## RESULTS

### Morphometry Identifies Two Subtypes of RGL Cells with Distinct Molecular Marker Expression

RGL cells were identified using two common transgenic mouse lines: the *GFAP*-GFP mice [25] and the *Nestin*-GFP mice [26]. In these mice, the GFP is expressed under the control of the human *GFAP* promoter or the *Nestin* promoter, respectively. At 8 weeks of age, mice were prepared for histology and immunostaining against GFP was used to amplify the fluorescent signal. In both mice, GFP<sup>+</sup> RGL cells displayed a prototypical morphology, including a nucleus located in the SGZ of the DG, a radial process extending through the GCL and extensively branching into the outer GCL and the molecular layer and a few basal processes extending towards the hilus [5–8] (Fig. 1A).

We measured the following parameters in 2472 *GFAP*-GFP<sup>+</sup> and 1150 *Nestin*-GFP<sup>+</sup> RGL cells: position of the soma relative to the basal limit of the GCL, length of the primary process, number of secondary branches stemming from the primary process, projected surface of the territory encompassed by the whole cell or only by the secondary apical arbor, and maximal width of the territory covered by the apical arbor (Fig. 1; Supporting Information Fig. 1A). On average, the soma of RGL cells was found within  $3.83 \pm 0.07$   $\mu$ m of the base of the GCL. The length of their primary radial process was  $75.82 \pm 0.34$   $\mu$ m; the main process had  $4.11 \pm 0.03$  branches; the secondary dendritic tree had a width of  $25.14 \pm 0.11$   $\mu$ m, covered a projected surface of  $569.51 \pm 36.83$   $\mu$ m<sup>2</sup> and the whole cell covered a surface area of  $1485.75 \pm 17.99$   $\mu$ m<sup>2</sup>. There was no interstrain difference in the morphology of RGL cells, indicating that these parameters did not depend on the genetic background or the reporter, but rather reflected common features of RGL cells. Notably, there was a great variation in both the length and the width among RGL cells, which defined two distinct populations: a first group of cells, which we named type  $\alpha$ , represented 75.46% of all RGL cells (73.8% in *Nestin*-GFP



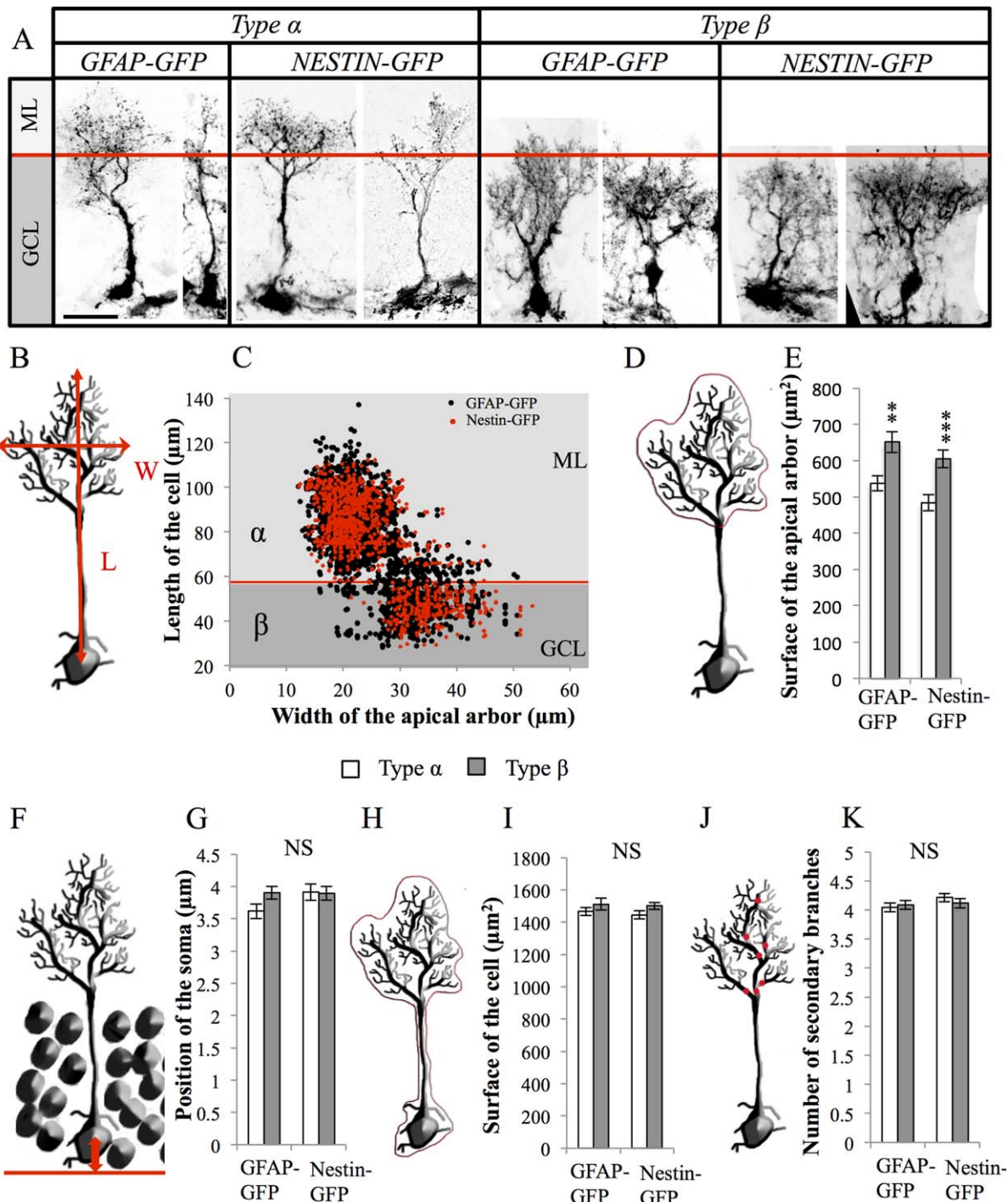


**Figure 1.** Morphometrical parameters of radial glia-like (RGL) cells. **(A):** Confocal maximal projection micrographs of types  $\alpha$  and  $\beta$  RGL cells in glial fibrillary acidic protein (GFAP)-green fluorescent protein (GFP) and *Nestin*-GFP mice. **(B):** Drawing of a RGL neural stem cell illustrating the measurements of length and width of the cell. **(C):** Scatter graph of all RGL cells analyzed morphometrically ( $n = 2472$  for GFAP-GFP mice and  $n = 1150$  for *Nestin*-GFP mice). **(D, E):** Schematic illustration (D) and histogram (E) of the projected surface of the dendritic arbor of secondary processes in types  $\alpha$  and  $\beta$  cells. **(F, G):** Schematic illustration (F) and histogram (G) of the position of the soma of type  $\alpha$  and the type  $\beta$  cells relative to the hilar border of the granule cell layer. **(H, I):** Schematic illustration (H) and histogram (I) of the total surface of types  $\alpha$  and  $\beta$  cells. **(J, K):** Drawing (J) and histogram (K) of the number of branches of the main process of types  $\alpha$  and  $\beta$  cells. Scale bar: 20  $\mu\text{m}$ . Bilateral Student's *t* test \*\*,  $p < 0.01$ ; \*\*\*,  $p < 0.001$ . Each value represents the mean  $\pm$  SEM. Abbreviations: GCL, granule cell layer; GFAP, glial fibrillary acidic protein; GFP, green fluorescent protein; ML, molecular layer.

mice and 76.2% in GFAP-GFP mice). They displayed a long radial process and a narrow arbor of secondary processes, which extended beyond the GCL, into the first third of the molecular layer. In contrast, a second group of cells named

type  $\beta$ , which represented 24.54% of all RGL cells (26.2% in *Nestin*-GFP mice and 23.8% in GFAP-GFP mice), displayed a short primary process (shorter than 58  $\mu\text{m}$ ) and a broad arbor of secondary processes, most of which did not extend

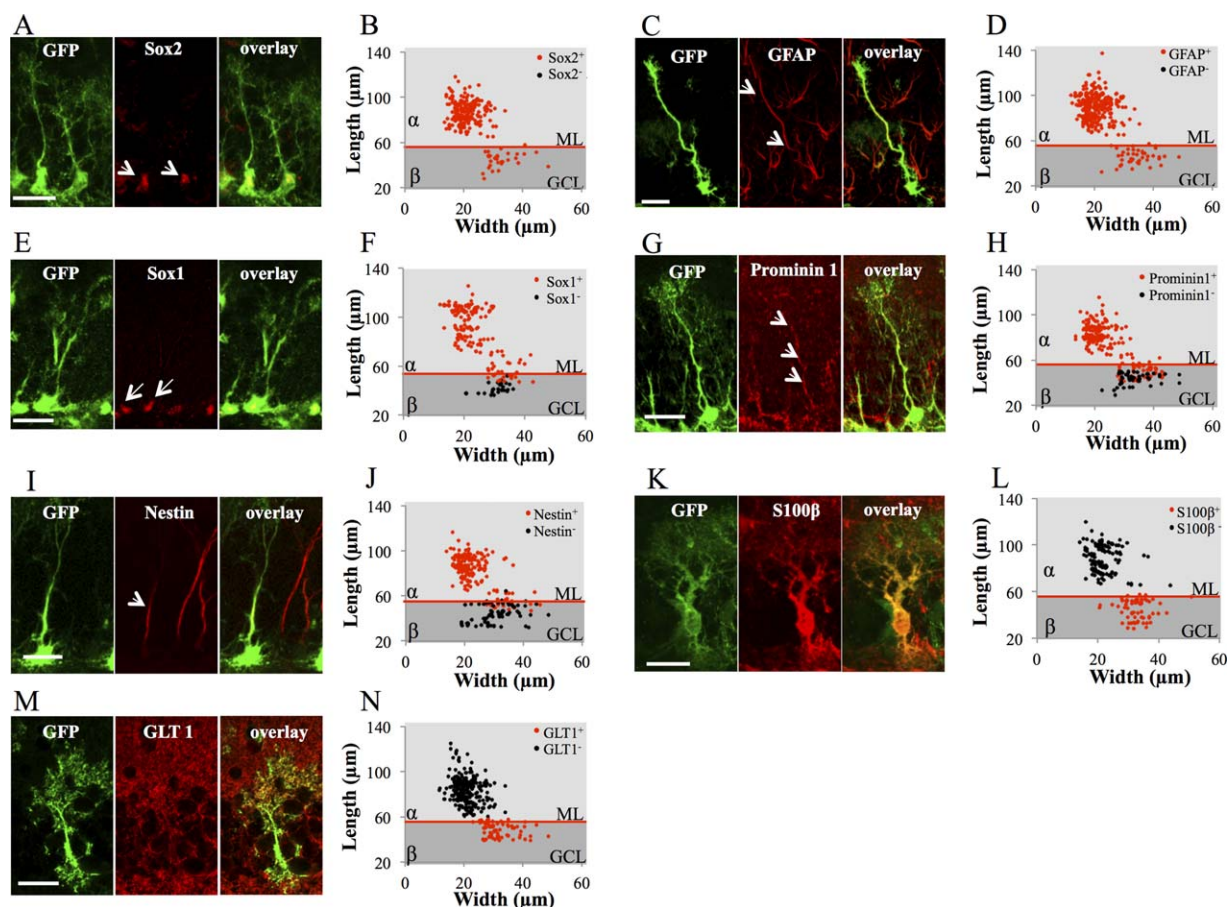


**Figure 2.** Molecular marker expression of type  $\alpha$  and type  $\beta$  cells. **(A):** Confocal maximal projection micrographs of glial fibrillary acidic protein (GFAP)-green fluorescent protein (GFP) radial glia-like (RGL) cells (green), immunostained for Sox2. **(B)** Scatter graphs representing the dimensions of RGL cells immunostained for Sox2. **(C):** Confocal maximal projection micrographs of GFAP-GFP RGL cells (green), immunostained for GFAP. **(D):** Scatter graphs representing the dimensions of RGL cells immunostained for GFAP. **(E):** Confocal maximal projection micrographs of GFAP-GFP RGL cells (green), immunostained for Sox1. **(F):** Scatter graphs representing the dimensions of RGL cells immunostained for Sox1. **(G):** Confocal maximal projection micrographs of GFAP-GFP RGL cells (green), immunostained for Prominin1. **(H):** Scatter graphs representing the dimensions of RGL cells immunostained for Prominin1. **(I):** Confocal maximal projection micrographs of GFAP-GFP RGL cells (green), immunostained for Nestin. **(J):** Scatter graphs representing the dimensions of RGL cells immunostained for Nestin. **(K):** Confocal maximal projection micrographs of GFAP-GFP RGL cells (green), immunostained for S100 $\beta$ . **(L):** Scatter graphs representing the dimensions of RGL cells immunostained for S100 $\beta$ . **(M):** Confocal maximal projection micrographs of GFAP-GFP RGL cells (green), immunostained for GLT1. **(N):** Scatter graphs representing the dimensions of RGL cells immunostained for GLT1. Scale bars = 20  $\mu$ m. Abbreviations: GCL, granule cell layer; GFAP, glial fibrillary acidic protein; GFP, green fluorescent protein; ML, molecular layer.

beyond the limit of the GCL (Fig. 1A–1C). Due to their broader arbor of processes, type  $\beta$  cells displayed an increased projected surface of their apical arbor (Fig. 1D–1E). Types  $\alpha$  and  $\beta$  cells were, however, similar in all other morphological criteria observed, regardless of the reporter mouse used to examine their morphology (Fig. 1F–1K). Thus, RGL cells are morphologically heterogeneous and are composed of two major morphotypes that can be clearly identified by the length of the primary process and the width of the arbor formed by the secondary processes.

We next examined the molecular identity of these two morphotypes using immunohistochemistry (Fig. 2; Supporting Information Fig. 1B). Types  $\alpha$  and  $\beta$  cells expressed the neural stem cell markers GFAP and Sox2. However, although the stem cell markers Sox1, Prominin 1, and Nestin were expressed in 100% of type  $\alpha$  cells, they were only expressed in a fraction of type  $\beta$  cells (49%, 32%, and 18%, respectively). Inversely, the astrocyte-specific glutamate transporter GLT1 and calcium binding protein S100 $\beta$  were expressed by all and virtually only type

$\beta$  cells. This indicates that a fraction of  $\beta$  cells coexpressed astrocytes-specific (GLT1, S100 $\beta$ ) and stem cell-specific markers (Prominin1, Nestin, and Sox1). Intriguingly, the morphology of type  $\beta$  cells expressing Sox1, Prominin1, or Nestin was different than from immunonegative type  $\beta$  cells: Sox1, Prominin1, and Nestin were present in the cells with the longest processes, indicating that the length of the process was associated with a “stem-like” molecular identity of these cells (Fig. 2E–2J).

Thus, types  $\alpha$  and  $\beta$  cells can be characterized by morphology and molecular markers: While type  $\alpha$  cells extend processes well into the molecular layer and express stem cell markers such as Sox2, Sox1, Nestin, GFAP, and Prominin1, type  $\beta$  cells are restricted into the GCL and express S100 $\beta$  and GLT1, accompanied by Prominin1, Sox1, and Nestin for the longest cells.

### Cellular Contacts with Niche Cells

The morphological differences between types  $\alpha$  and  $\beta$  cells may enable them to interact with distinct niche cells which, in turn, may underlie different regulation mechanisms of their



activity. To examine the contacts between RGL cells and their cellular environment, as well as their relevance to proliferation, we examined mice in standard housing conditions and in

cages containing a running wheel, a condition of voluntary exercise known to increase proliferation [4] (Fig. 3). After 2 weeks of exposure to a running wheel (or the same housing

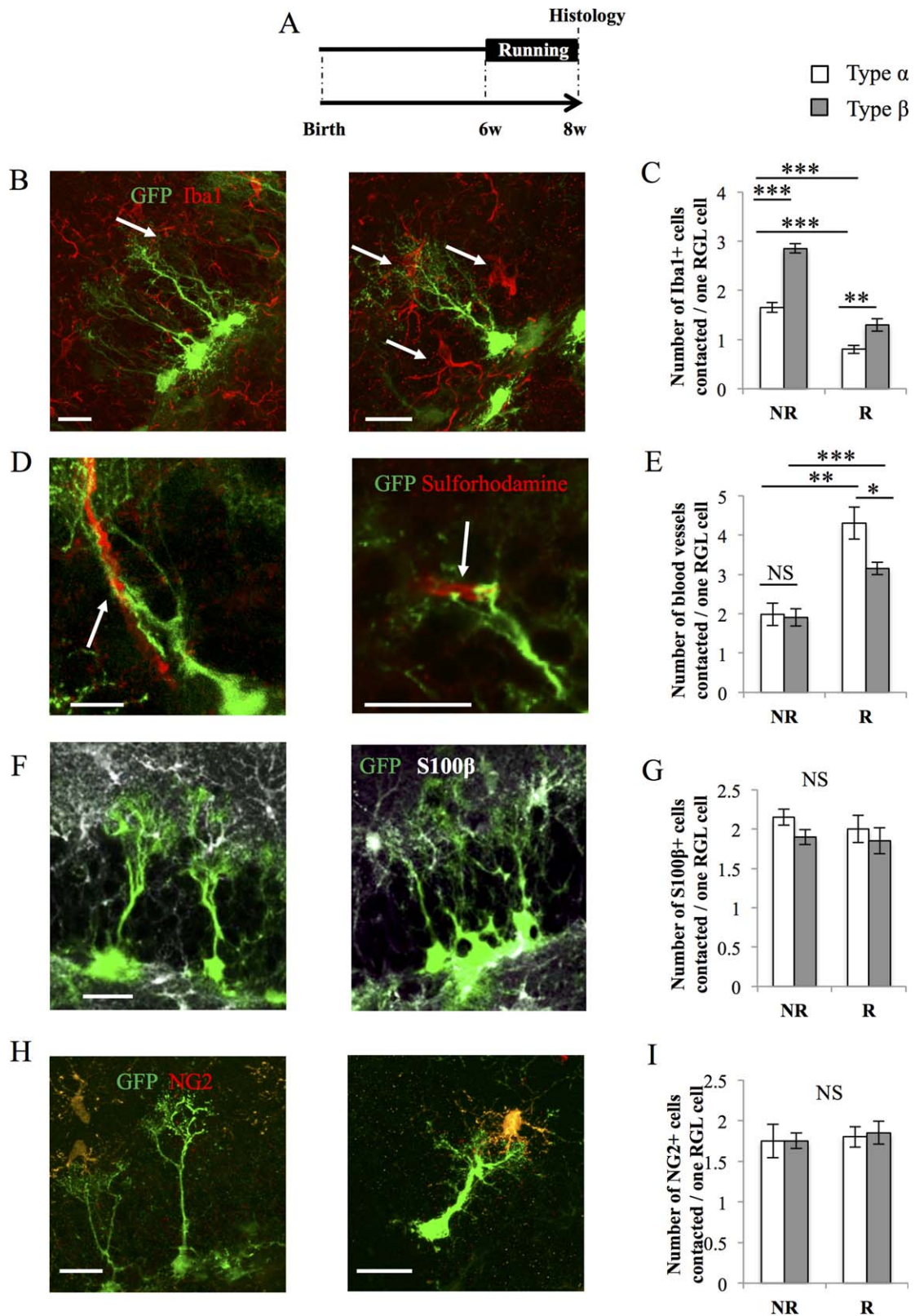


Figure 3.

cage without a running wheel), all mice were killed and immunohistochemistry was used to identify microglia (Iba1), astrocytes (S100 $\beta$ ), and oligodendrocyte progenitor cells (NG2). Sulforhodamine 101 was used to identify blood vessels.

Under basal housing conditions (NR), individual RGL cell types contacted on average 2 blood vessels, 2.5 astrocytes, and 1.7 oligodendrocyte precursors, independently of their morphotype. In contrast, type  $\beta$  cells contacted significantly more microglia cells (2.8 microglia per type  $\beta$  cell) than by type  $\alpha$  cells (1.6 microglia per type  $\alpha$  cell, Fig. 3B–3I). The majority of the contacts with microglia occurred on the main process or the secondary processes of RGL cells, but no contact was observed on the soma (Fig. 3B). In running conditions (R), both types  $\alpha$  and  $\beta$  cells contacted fewer microglia and more blood vessels than in nonrunning conditions. To test whether running affected RGL cells or niche cells, we examined the morphology of niche cells in running conditions. Consistent with our previous observations [22], running decreased the number of Iba1-expressing microglia, but increased the size of their territory and the number of branches (Supporting Information Fig. 2A–2C). Inversely, running increased the number and/or the size of blood vessels in the dentate gyrus, as reflected by increased number of pixels labeled by Sulforhodamine 101 (Supporting Information Fig. 2D–2F).

These results indicate that type  $\beta$  cells preferentially contacted microglia and that voluntary running increased the number of blood vessels and decreased the number of microglia, therefore, interfering with the contacts between types  $\alpha$  and  $\beta$  cells with the niche.

### Types $\alpha$ and $\beta$ Cells Respond Differently to Proliferative Stimuli

The proliferation of adult neural stem/progenitor cells is regulated by external stimuli and is increased by voluntary running [4] and decreases with aging [29]. To examine whether these conditions affected the number or the morphology of types  $\alpha$  and  $\beta$  cells, 16 GFAP-GFP mice were divided in four experimental groups: young adult mice (8 weeks of age; Y) and older mice (8 months of age; O), that were housed individually in standard cages in presence (R) or absence (NR) of a running wheel for 2 weeks (Fig. 4A, 4 mice per group). The total number of RGL cells was significantly decreased by aging and increased by running (Fig. 4B, 4E). Similarly, voluntary running increased, whereas aging decreased the number of

type  $\alpha$  cells (Fig. 4C). In contrast, neither running, nor aging had any effect on the total number of type  $\beta$  cells (Fig. 4D). As a result, when the relative proportions of types  $\alpha$  and  $\beta$  cells were calculated, Y, YR, and OR mice displayed mainly type  $\alpha$  cells (66.6%, 80.6%, and 58%, respectively), whereas type  $\beta$  cells were more frequently observed on O mice (89%, Fig. 4B–4E). The length and width of types  $\alpha$  and  $\beta$  cells were not modified by running or aging (Supporting Information Fig. 3). Thus, aging and exercise strongly modified the number of type  $\alpha$  cells, but not the number of type  $\beta$  cells.

We next examined whether the pharmacological stimulation of adult neurogenesis cells may have a similar effect on the different morphotypes of cells. We recently reported that the administration of the NMDA receptor co-agonist D-serine increases the density of RGL stem cells [30]. Here, we repeated this experiment and injected four mice with D-serine (daily intraperitoneal injections 50 mg/kg, for 8 days during the eighth week of life) and four mice with the same volume of saline. All mice were examined 1 day after the last injection (Fig. 5A). Similarly to our previous observations, D-serine increased the total number of RGL cells. This increase was mediated by an increase in both the number of type  $\alpha$  cells (120% increase) and type  $\beta$  cells (160% increase, Fig. 5B–5E). Moreover, the effect of D-serine was specific to RGL cells, since D-serine treatment did not change the number of GFAP-immunolabeled stellar astrocytes in the dentate gyrus [30]. To examine whether D-serine activated the proliferation of types  $\alpha$  and  $\beta$  cells, we immunostained hippocampal slices for the cell proliferation marker Ki-67. Ki-67 is a nuclear protein associated with proliferation that is expressed during all active phases of the cell cycle. Of 545 cells analyzed, Ki-67 was expressed in about 10.45% of type  $\alpha$  cells, but was not expressed in type  $\beta$  cells (Fig. 5F–5G). D-Serine significantly increased the proportion of Ki-67-expressing type  $\alpha$  cells as compared to the proportion found in control, nontreated mice ( $p < 0.01$ , Fig. 6C).

Thus, D-serine increased the proliferation of type  $\alpha$  and resulted in increased number of types  $\alpha$  and  $\beta$  cells, but did not affect the proliferation of type  $\beta$  cells.

### Proliferative Properties of Types $\alpha$ and $\beta$ Cells

To examine the proliferative properties of types  $\alpha$  and  $\beta$  cells, we immunostained hippocampal slices for the cell proliferation marker Ki-67 (Fig. 6A–6C). Of 1555 cells analyzed, Ki-67

**Figure 3.** Type  $\alpha$  and  $\beta$  cells contact niche-forming cells. **(A)**: Experimental timeline. GFAP-GFP mice were housed in normal cages (NR) or in cages containing a running wheel (R) for 2 weeks before histological analysis. **(B)**: Confocal maximal projection micrographs of radial glia-like (RGL) cells (green) and Iba1-immunostained microglia (red). **(C)**: Histogram of the average number of microglia cells contacted per RGL cell. Type  $\beta$  cells contact more microglia than type  $\alpha$  cells (one-way analysis of variance [ANOVA]  $F(3, 15) = 73.12$ ;  $p < 0.001$ . Post hoc bilateral Student's  $t$  test: No Run [type  $\alpha$  vs. type  $\beta$ ]  $p < 0.001$ , Run [type  $\alpha$  vs. type  $\beta$ ]  $p < 0.01$ ). Two weeks of running decrease the interaction of microglia with both types  $\alpha$  and  $\beta$  cells (post hoc bilateral Student's  $t$  test: type  $\alpha$  [No Run vs. Run]  $p < 0.001$ , type  $\beta$  [No Run vs. Run]  $p < 0.001$ ). **(D)**: Confocal maximal projection micrographs of RGL cells (green) and blood vessels, identified with Sulforhodamine (red). **(E)**: Histogram of the number of blood vessels contacted per RGL stem cell. In sedentary mice, there is no difference between type  $\alpha$  of a type  $\beta$  cell in sedentary conditions (one-way ANOVA  $F(3, 15) = 16.10$ ;  $p < 0.001$ . Post hoc bilateral Student's  $t$  test: No Run [type  $\alpha$  vs. type  $\beta$ ]  $p = 0.84$ ). In running mice, blood vessel are more contacted by type  $\alpha$  than type  $\beta$  cells (post hoc bilateral Student's  $t$  test: Run [type  $\alpha$  vs. type  $\beta$ ]  $p < 0.05$ ). Running, significantly increased the number of blood vessels contacted by both cell types (one-way ANOVA  $F(3, 15) = 16.10$ ;  $p < 0.001$ . Post hoc bilateral Student's  $t$  test: type  $\alpha$  [No Run vs. Run]  $p < 0.001$ , type  $\beta$  [No Run vs. Run]  $p < 0.01$ ). **(F)**: Confocal maximal projection micrographs of RGL cells (green) and S100 $\beta$ -immunostained astrocytes (white). **(G)**: Histogram of the number of astrocytes contacted per type  $\alpha$  or type  $\beta$  cells. **(H)**: Confocal maximal projection micrographs of RGL cells (green) and NG2-immunostained oligodendrocyte precursors cells (red). **(I)**: Histogram of the number of oligodendrocyte precursor cells contacted by types  $\alpha$  or  $\beta$  cells. Scale bars = 20  $\mu\text{m}$ .  $N = 4$  animals per group. Each value represents the mean  $\pm$  SEM. \*,  $p < 0.05$ ; \*\*,  $p < 0.01$ ; \*\*\*,  $p < 0.001$ . Abbreviations: GFP, green fluorescent protein; RGL, radial glia-like.



was expressed in about 5% of type  $\alpha$  cells, but was not expressed in type  $\beta$  cells. Notably, type  $\alpha$ -Ki-67<sup>+</sup> cells displayed a longer process than type  $\alpha$ -Ki-67<sup>-</sup> cells (Fig. 6D). These results suggest that type  $\beta$  cells do not proliferate and

support the possibility that the RGL cells' processes may play a role in proliferation.

To further examine cell proliferation, we performed pulse chase experiments with three different BrdU injection

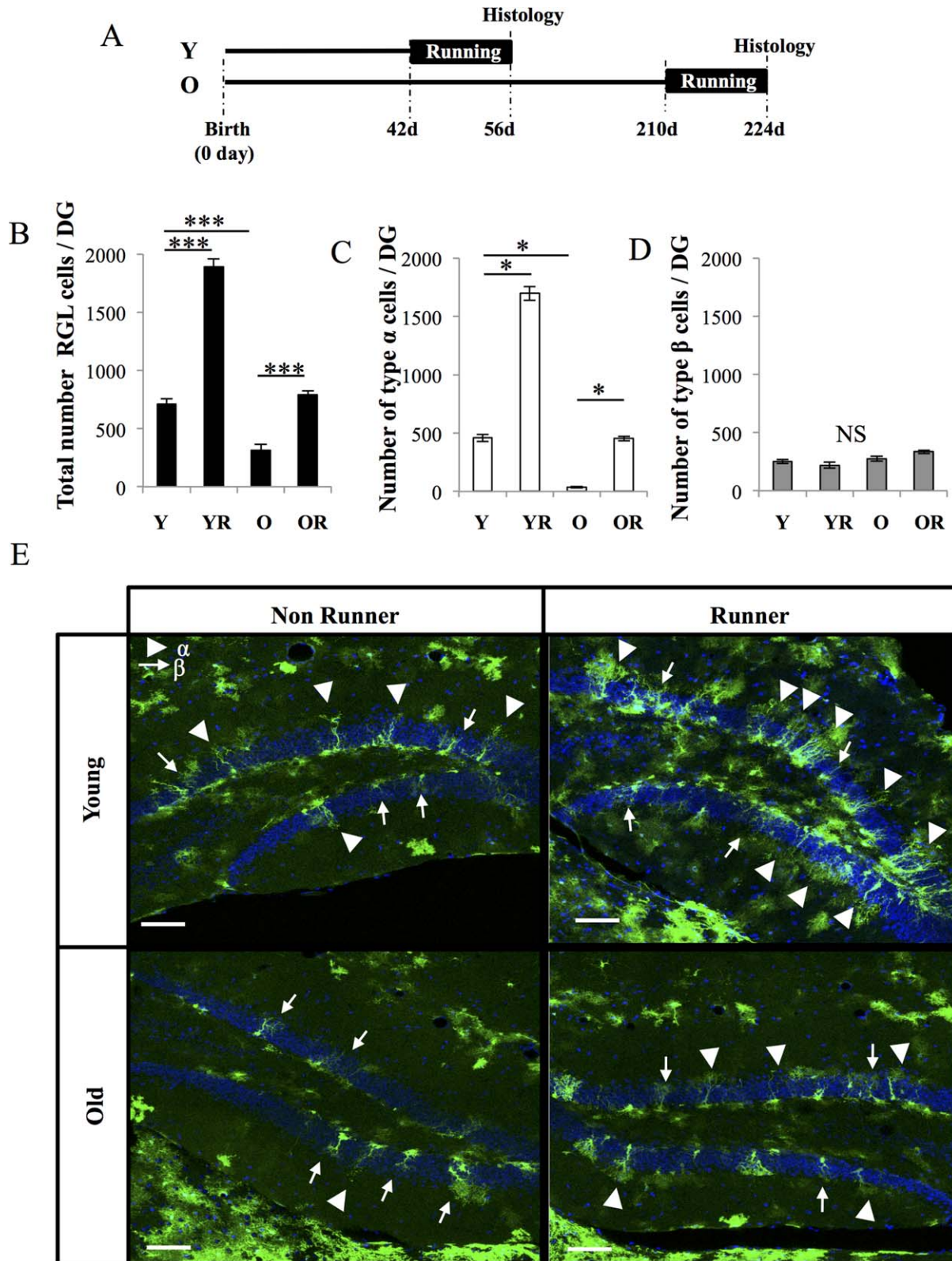


Figure 4.



protocols. By incorporating into the nascent DNA strand during mitosis, BrdU enables the labeling of dividing cells and their progenies. First, we injected mice with BrdU ( $1 \times 100$  mg/kg) and killed the mice 2 hours after the last BrdU-injection (Fig. 6E). This protocol enables the labeling of fast dividing progenitor cells, however, BrdU was incorporated in 3.9% type  $\alpha$  cells, but was absent from type  $\beta$  cells (Fig. 6F). Then we injected mice with BrdU ( $3 \times 100$  mg/kg) and killed the mice 24 hours after the last BrdU-injection (Fig. 6G–6I). Of 500 cells, BrdU was incorporated in 3.64% of type  $\alpha$  and 0.4% of type  $\beta$ . Moreover, the BrdU<sup>+</sup> type  $\beta$  cells were closely attached to BrdU<sup>+</sup> type  $\alpha$  cells (Fig. 6H). In a third experiment, we injected mice with BrdU daily for 8 days (100 mg/kg) and killed the mice 1 day after the last BrdU-injection (Fig. 6J). Both types  $\alpha$  and  $\beta$  cell types incorporated BrdU, although type  $\alpha$  cells to a much greater extent than type  $\beta$  cells (Fig. 6K–6L, 527 cells analyzed, BrdU<sup>+</sup> type  $\alpha$ : 5.69%, BrdU<sup>+</sup> type  $\beta$ : 0.94%). In contrast with Ki-67 labeling, the proportion of BrdU-labeled cells did not correlate with the dimensions of the cells (Fig. 6K).

Taken together, these results suggest that type  $\beta$  cells do not proliferate but are generated by the division of type  $\alpha$  cells. To further examine this possibility, we performed a clonal analysis.

#### Fate Analysis of Type $\alpha$ and Type $\beta$ Cells

To examine the fate of individual RGL cells, we used two transgenic mice, the *GFAP::CreER<sup>T2</sup>* and the *Nestin::CreER<sup>T2</sup>*. We crossed the *Nestin::CreER<sup>T2</sup>* transgenic mouse (expressing the tamoxifen-inducible Cre recombinase under the control of the Nestin promoter) with reporter mice (ROSA-tdTomato or Z/EG<sup>f/+</sup>) (Fig. 7A). The *GFAP::CreER<sup>T2</sup>* was crossed with the ROSA-YFP reporter mouse. A minimal tamoxifen injection resulted in the sparse labelling of adult neural stem cells, thereby enabling the identification and morphological analysis of individual clones [14]. To examine clones shortly after division, we killed the animals 1, 2, 3, or 7 days after tamoxifen injection (dpi, Fig. 7B).

In *Nestin::CreER<sup>T2</sup>* mice, we didn't detect any difference between the two reporter mice, therefore we combine the results of both mice. All clones are described and shown in Supporting Information Figures 4–6. Across all time points, we examined 227 clones that contained at least one RGL cell, which were most frequently accompanied by a neuronal progenitor/type 2 cell (N) or an astrocyte (A, Fig. 7; Supporting Information Fig. 4A). Astrocytes were defined by their typical stellar astrocytes morphology and their identity was confirmed by immunohistology against GFAP. Neuronal progenitor/type 2 cells were identified based on the absence of GFAP immunoreactivity and their short processes oriented horizon-

tally or radially (Supporting Information Fig. 6). The most parsimonious clonal relationships between cells present in each clones revealed that 26.9% of the clones displayed an isolated RGL cell (all of which consisted of type  $\alpha$  cells), suggesting no division, 37% of the clones divided once and 36.1% divided twice (Fig. 7F–7H; Supporting Information Fig. 4A). Of the 166 clones that divided at least once, 51.8% generated a neural progenitor/type 2 cell, 24.7% generated an astrocyte and 77.7% generated a RGL cell (including clones that contained neurons or astrocytes, Fig. 7C). Type  $\beta$  cells were more often observed in clones that contained astrocytes than in clones containing neurons, suggesting that they originated from  $\alpha$  cells that were prone to gliogenesis (Fig. 7C). Finally, among the 129 clones in which a new RGL cell was observed, 44% generated 1 type  $\beta$  cell, 7% generated 2 type  $\beta$  cells and 49% generated a new type  $\alpha$  cell (Fig. 7D). Thus, of 166 clones that divided at least once, 75 new type  $\beta$  cells and 63 new type  $\alpha$  cells were generated (Fig. 7E; see summary table on Supporting Information Fig. 5A).

In *GFAP::CreER<sup>T2</sup>* mice, across all time points, we examined 93 clones. Similarly to *Nestin::CreER<sup>T2</sup>* mice, 5.3% of the clones did not divide, 46.3% divided once, and 48.4% divided twice (Supporting Information Figs. 4B, 5B). Of the 88 clones that divided, 56.8% generated a neuronal progenitor/type 2 cell, 12.5% generated and astrocyte, and 81.8% generated a RGL cell. Moreover similarly to *Nestin::Cre* mice, type  $\beta$  cells were more often observed in clones that contained astrocytes.

Thus, type  $\alpha$  cells undergo numerous modes of division to generate type  $\alpha$  cells, type  $\beta$  cells, neurons and astrocytes and new type  $\beta$  cells are frequently generated upon division of type  $\alpha$  cells.

#### DISCUSSION

Using a combination of morphometry, immunohistochemistry and clonal analysis, we found that two morphotypes of RGL cells coexist in the SGZ of the dentate gyrus, which can be characterized by two simple morphological features, the length of the primary process and the width of the arbor of secondary processes: Type  $\alpha$  cells represented 76.21% of RGL cells and displayed a long radial process and a narrow arbor of secondary processes extending well into the first third of the molecular layer. These cells expressed stem cell markers, self-replicated and produced neurons, astrocytes and type  $\beta$  cells. Their total number was also greatly increased by voluntary running and D-serine administration and decreased by aging. In contrast, type  $\beta$  cells (which represented 23.79% of all RGL cells) had a short radial process and their secondary processes branched mainly in the GCL. Marker expression

**Figure 4.** Number of type  $\alpha$  but not type  $\beta$  cells are changed by running and aging. **(A):** Experimental timeline. GFAP-GFP mice were exposed to sedentary housing or cages with a running wheel (R), starting either at 42 days (Y) or 210 days (O) after birth. Mice were killed and examined 2 weeks after exposure to running wheel cages. **(B):** Histogram of the total number of radial glia-like (RGL) cells in the dentate gyrus. Two-way analysis of variance (ANOVA) test showed that there is interaction between aging and running ( $F(1, 12) = 35.50$ ;  $p < 0.001$ ). The total number of RGL cells was significantly decreased with aging post hoc bilateral Student's *t* test (Y vs. O;  $p < 0.001$ ) and increased by running (one-way ANOVA  $F(3, 15) = 127.32$ ;  $p < 0.001$ ). Post hoc bilateral Student's *t* test (Y vs. YR  $p < 0.001$ , O vs. OR  $p < 0.001$ ). **(C):** Histogram of the number of type  $\alpha$  cells in the dentate gyrus. Voluntary running increased, whereas aging decreased the number of type  $\alpha$  cells Kruskal-Wallis test  $p < 0.01$ . Post hoc Wilcoxon test (Y vs. O  $p < 0.05$ ; Kruskal-Wallis test  $p < 0.01$ ). Post hoc Wilcoxon test (Y vs. YR  $p < 0.05$ , O vs. OR  $p < 0.05$ ). **(D):** Histogram of the number of type  $\beta$  cells in the dentate gyrus. **(E):** Confocal maximal projection micrographs of hippocampal sections. Scale bars = 100  $\mu$ m. \*,  $p < 0.05$ ; \*\*\*,  $p < 0.001$ , NS: Not significant. Abbreviations: DG, Dentate Gyrus; RGL, radial glia-like.

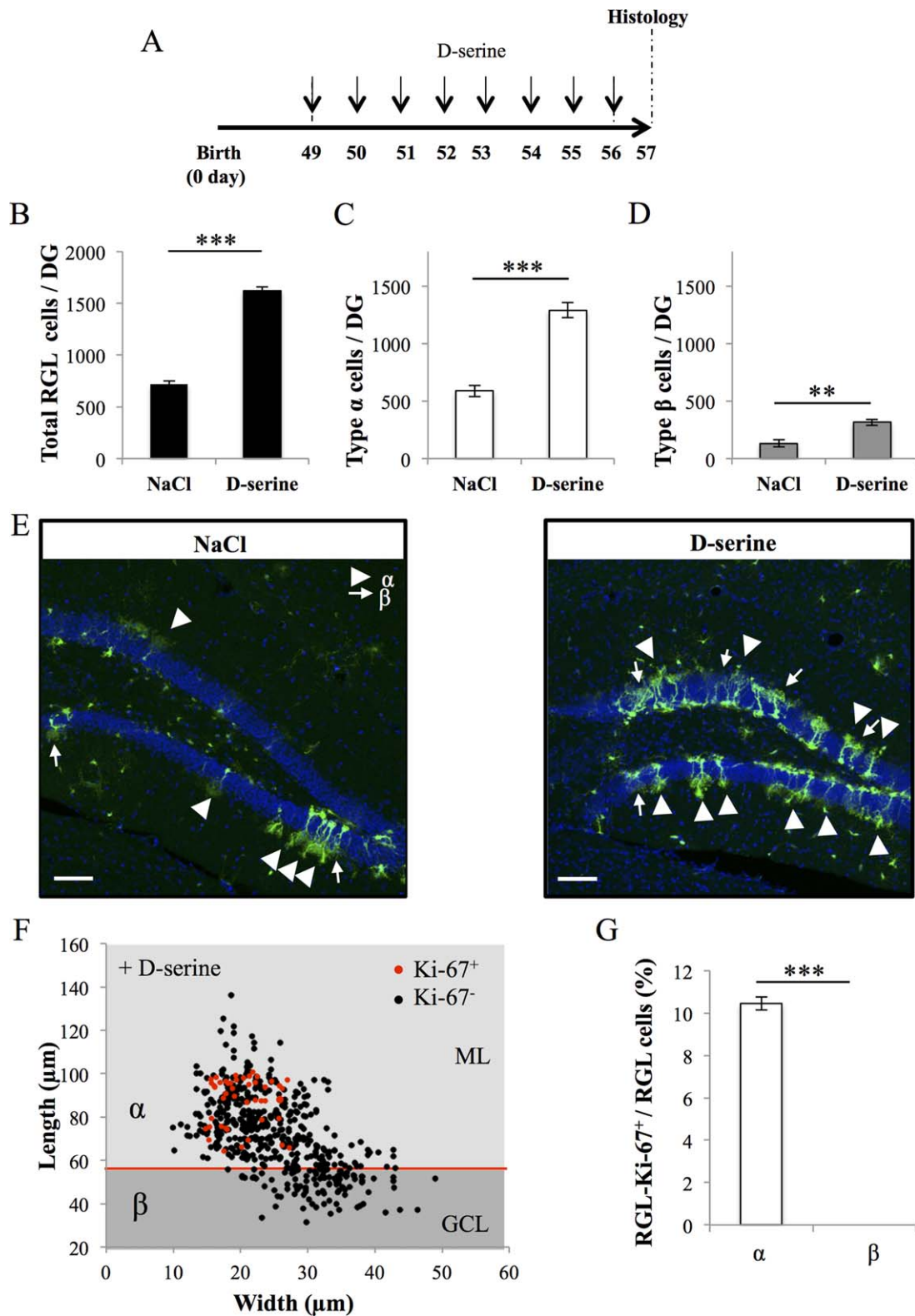


**Figure 5.** Number of types  $\alpha$  and  $\beta$  cells are increased by D-serine injection. **(A):** Experimental timeline: Nestin-GFP mice were injected with D-serine, daily for 8 days, starting at 49 days after birth and were killed 1 day after the last D-serine injection. **(B):** Histogram of the total number of radial glia-like (RGL) cells in the dentate gyrus (bilateral Student's *t* test  $p < 0.001$ ). **(C):** Histogram of the number of type  $\alpha$  cells in the dentate gyrus (bilateral Student's *t* test  $p < 0.001$ ). **(D):** Histogram of the number of the type  $\beta$  cells in the dentate gyrus (bilateral Student's *t* test  $p < 0.01$ ). **(E):** Confocal maximal projection micrographs of hippocampal sections. **(F):** Scatter graph of RGL cells dimensions. Red dots: Ki-67<sup>+</sup> cells  $N = 45$ , black dots Ki-67<sup>-</sup> cells  $N = 500$ . **(G):** Histogram showing the percentage of types  $\alpha$  and  $\beta$  cells expressing Ki-67. Bilateral Student's *t* test. Scale bars = 100  $\mu$ m.  $N = 4$  animals per group. Each value represents the mean  $\pm$  SEM. \*\*,  $p < 0.01$ ; \*\*\*,  $p < 0.001$ . Abbreviations: DG, Dentate Gyrus; GCL, granule cell layer; ML, molecular layer; RGL, radial glia-like.

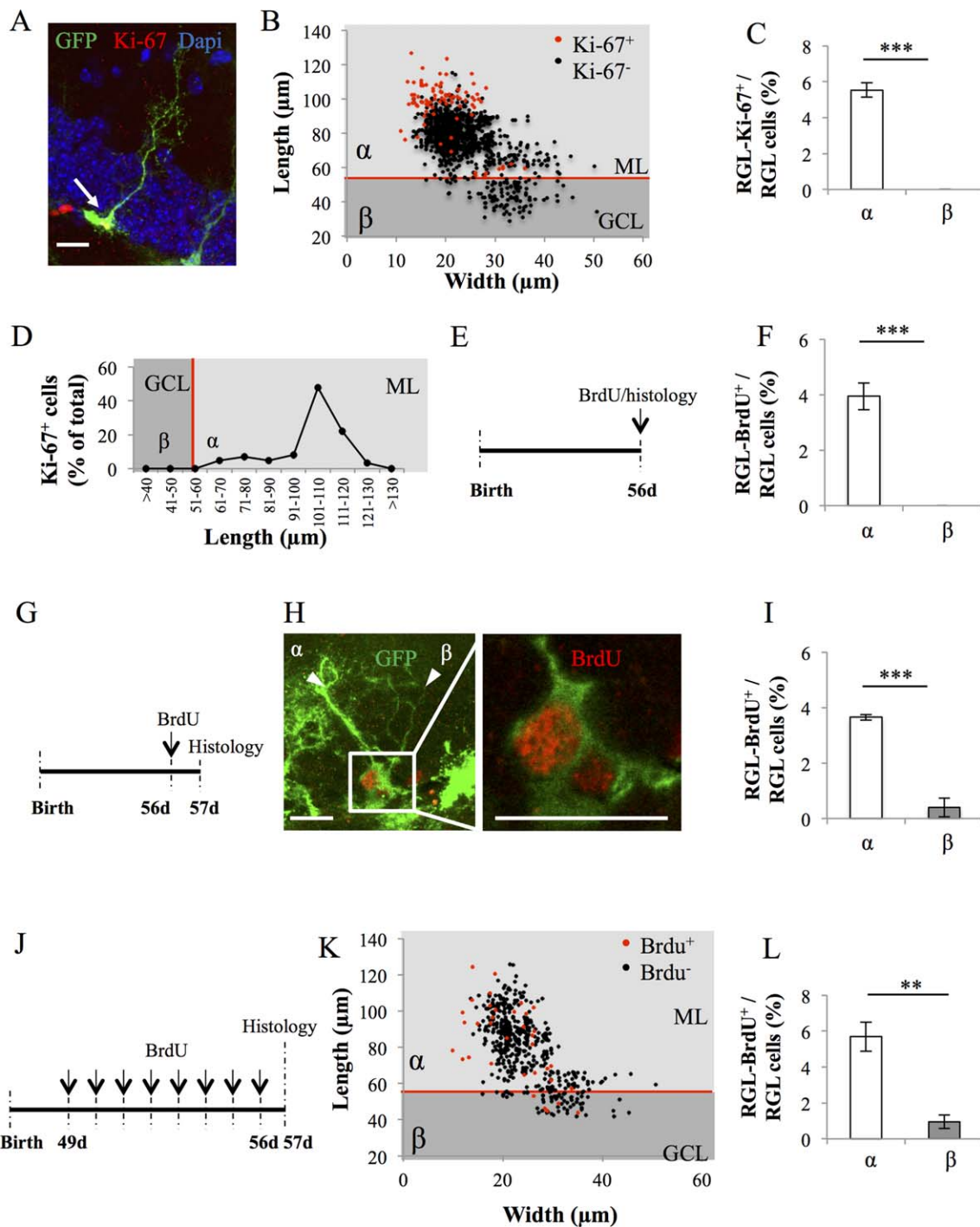


**Figure 6.** Proliferative properties of types  $\alpha$  and  $\beta$  cells in GFAP-GFP mice. **(A):** Confocal maximal projection micrograph of radial glia-like (RGL) cell (green), immunostained for Ki-67 (red). **(B):** Scatter graph of RGL cell dimensions. Red dots: Ki-67<sup>+</sup> cells  $N = 86$ , black dots Ki-67<sup>-</sup> cells  $N = 1469$ . **(C):** Histogram showing the percentage of types  $\alpha$  and  $\beta$  cells expressing Ki-67. Bilateral Student's  $t$  test. **(D):** Line graph representing the proportion of RGL cells expressing Ki-67 according to their length. **(E):** Experimental timeline: mice were injected intraperitoneally (i.p.) at doses of 100 mg/kg in saline, three times at 2-hour intervals and killed 2 hours after the last injection. **(F):** Histogram showing the percentage of types  $\alpha$  and  $\beta$  cells expressing bromodeoxyuridine (BrdU).  $N = 500$  cells. Bilateral Student's  $t$  test. **(G):** Experimental timeline: mice were injected i.p. at doses of 100 mg/kg in saline, three times at 2-hour intervals and killed 24 hours after the last injection. **(H):** Confocal maximal projection micrograph of types  $\alpha$  and  $\beta$  cells expressing BrdU. Confocal micrograph of one focal plan showing the immunoreactive cells Scale bar:  $20 \mu\text{m}$  **(I)** Histogram showing the percentage of types  $\alpha$  and  $\beta$  cells expressing BrdU.  $N = 500$  cells. Bilateral Student's  $t$  test. **(J):** Experimental timeline: Mice were injected daily with BrdU for 8 consecutive days, starting at 49 days after birth. One day after the last injection, they were killed and prepared for histology. **(K):** Scatter graphs representing the dimensions of RGL cells after immunostaining for BrdU (red dots: BrdU<sup>+</sup> cells  $N = 35$ , black dots BrdU<sup>-</sup> cells  $N = 492$ ) **(L):** Histogram showing the proportion of types  $\alpha$  and  $\beta$  cells that incorporated BrdU. Bilateral Student's  $t$  test. Scale bar:  $20 \mu\text{m}$ . Each value represents the mean  $\pm$  SEM. \*\*,  $p < 0.01$  \*\*\*,  $p < 0.001$ . Abbreviations: BrdU, bromodeoxyuridine; GCL, granule cell layer; GFP, green fluorescent protein; ML, molecular layer; RGL, radial glia-like.



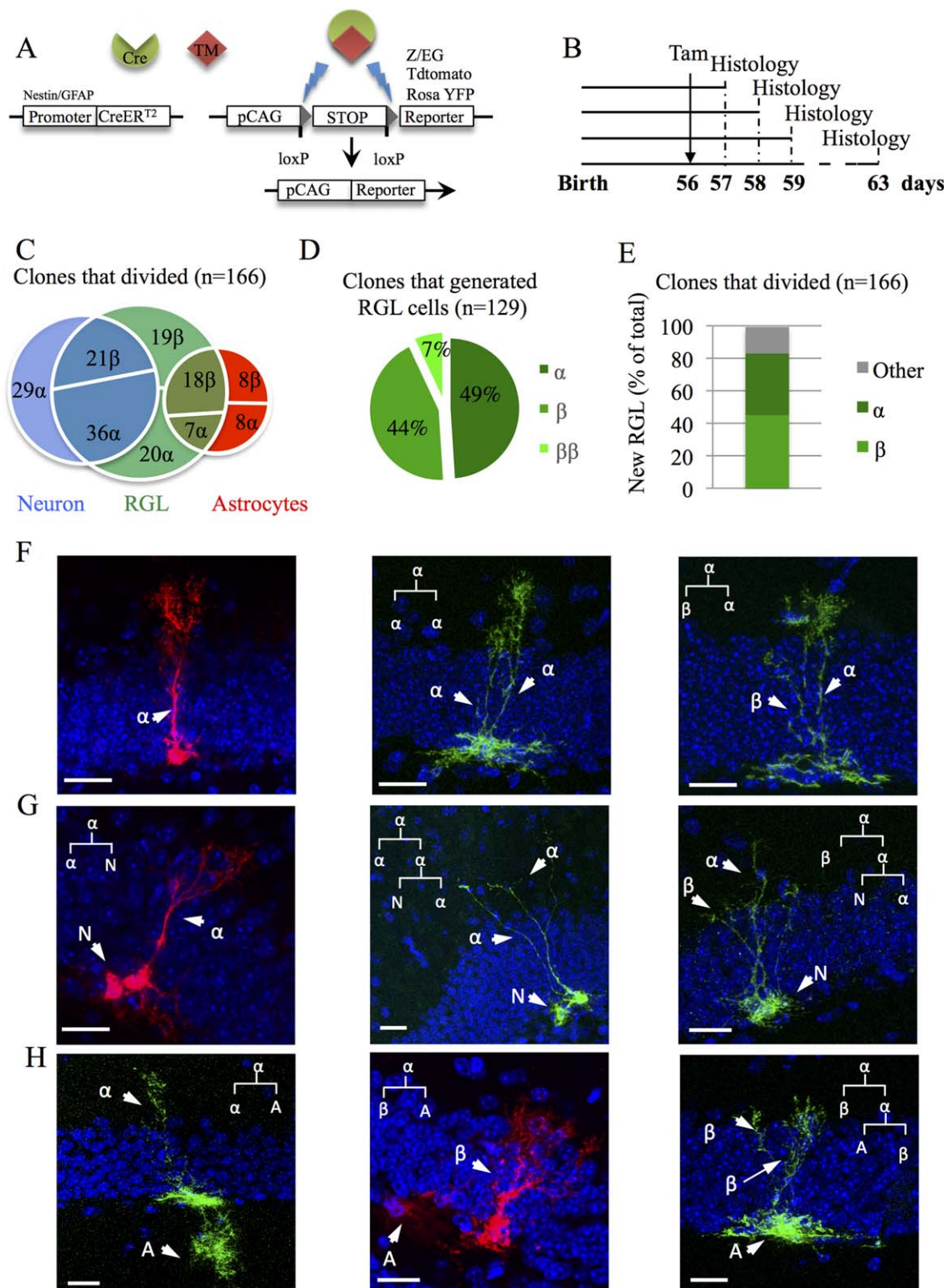


**Figure 7.** Clonal analysis of types  $\alpha$  and  $\beta$  cells. **(A):** Breeding scheme for clonal analysis: *Nestin-CreER<sup>T2</sup>* mice were crossed to fluorescent reporter mice *Rosa-tdTomato* or *Z/EG<sup>f/+</sup>* and glial fibrillary acidic protein (*GFAP*):*CreER<sup>T2</sup>* were crossed with *Rosa-YFP* reporter mice **(B):** Experimental timeline: *Nestin::CreERT2* x *Rosa-tdTomato* or *Z/EG<sup>f/+</sup>* mice were injected with tamoxifen (Tam) at 56 days after birth and killed 1, 2, 3, and 7 day after Tam injection (dpi). **(C):** Venn diagram showing the percentage of clones that generated neurons, astrocytes, or radial glia-like (RGL) cells out of all clones that divided. **(D):** Pie chart representing the distribution of newly generated RGL cells among clones that generated new RGL cells. **(E):** Histogram showing the percentage of newly generated RGL among the total number of dividing clones. **(F–H):** Confocal micrographs of different clones with hypothetical (linkage) tree of fate. Clones generated either only new RGL cells (F), neuronal progenitor/type 2 cell (G) or astrocytes (H). (N = type 2/neuronal progenitor, A = astrocyte). Scale bars = 20  $\mu$ m. Abbreviation: RGL, radial glia-like.

analyses revealed the coexpression of astrocytic and stem cell markers. These cells did not proliferate and their population size did not change upon aging or exercise, but was increased by D-serine administration. Together, these results reveal the coexistence within the dentate gyrus, of two populations of cells with prototypical morphology of RGL stem cells, but with radically different morphological and functional properties.

The strong association between morphology and function of RGL cells suggests that the processes of RGL cells play a potential role in regulating their activity. The shorter processes of type  $\beta$  cells do not reach the molecular layer. Although the role of the highly branched and long processes of RGL stem cells is still unclear, our results support the view that these processes establish specific contacts with the neurogenic niche [16]. We identified here that both types  $\alpha$  and  $\beta$  cells established direct cellular contacts with several cell types of the neurogenic niche, including but not restricted to microglia, astrocytes, NG2-expressing glia, and blood vessels. Direct signaling with these cells are known to participate to the regulation stem cell proliferation and fate determination, as has recently been shown for astrocytes [24], blood vessels [18, 31], or microglia [22, 23]. Contacts with microglia seems of particular relevance to the identity of type  $\beta$  cells, since they contacted significantly more microglia than type  $\alpha$  cells in normal (sedentary) conditions. The presence of microglia in the dentate gyrus has been associated with inflammation, which can reduce neurogenesis by the production of cytokines [32]. In absence of inflammation, microglia contribute to the phagocytosis of early progenitors undergoing apoptotic elimination during the neuroprogenitors to neuroblasts transition [23]. However, we found no evidence of microglial engulfment of type  $\alpha$  or type  $\beta$  cells and the contacts that these cells established with microglia occurred mainly on the fine, secondary processes rather than on the soma, as has been described for phagocytic engulfment [23]. Our results therefore are consistent with the view that microglia may regulate RGL stem cell proliferation using paracrine or juxtacrine signaling, independently from inflammatory pathway [22]. Consistently, running modified the number and the structure of microglia cells (Supporting Information Fig. 2) and resulted in increased proliferation of type  $\alpha$  cells (Fig. 3). Thus, cellular contacts established by RGL stem cells may be involved in the regulation of their proliferation. This possibility calls for a further examination of the specific contacts they form in the molecular layer, especially with microglia and blood vessels, with higher resolution imaging such as electron microscopy. Furthermore, whether the increased contacts between microglia and type  $\beta$  are a cause or consequence of their dormancy remains uncertain and this question will require further investigation with the use of live-cell imaging.

Type  $\alpha$  cells display all characteristics of RGL stem cells [11, 14, 33, 34], but the identity of type  $\beta$  cells is less clear. Morphology and molecular marker expression suggest that these cells are intermediate between quiescent RGL stem cells and stellate, protoplasmic astrocytes. Indeed, type  $\beta$  cells express both stem cell markers such as Nestin, Prominin 1, Sox 1, and Sox 2, but also the mature astrocytic marker S100 $\beta$  and GLT1, which are normally not expressed in RGL stem cells [11]. Similarly, the morphology of type  $\beta$  cells is less polarized than type  $\alpha$  cells, with shorter radial process and larger branches of secondary processes than type  $\alpha$  cells,

but not quite as round and branched as protoplasmic astrocytes. Furthermore, the absence of expression of the essential cell cycle marker Ki-67 from type  $\beta$  cells (Fig. 6A–6C), even upon activation by D-serine (Fig. 5F–5G) and the lack of BrdU incorporation in short (2 hours) pulses (Fig. 6D–6F) indicates that type  $\beta$  cells do not divide. Instead, we propose that type  $\beta$  cells are formed upon the division of type  $\alpha$  cells. Consistent with this hypothesis, clonal analysis shows that type  $\beta$  cells were never found alone and all type  $\beta$  cells that incorporated BrdU after a 24 hours pulse were found apposed to a type  $\alpha$  cell (Fig. 6G–6I). Although we cannot exclude that type  $\beta$  cells may represent a highly quiescent pool of RGL stem cells which may be converted into type  $\alpha$  cells upon proper stimulation, this possibility is not supported by our results. Alternatively, type  $\beta$  cells may represent a transitional morphology of type  $\alpha$  cells undergoing conversion into astrocytes, as has been proposed during aging [14, 33] or epilepsy-induced hyperactivation [35] (See schematic model in Supporting Information Fig. 7). In favor of this possibility, long primary processes in RGL cells were associated with Ki-67 expression (Figs. 5F, 6D) and type  $\beta$  cells that expressed stem cell markers (Sox 1, Prominin 1, and Nestin), had a longer primary process than cells not expressing these markers (Fig. 2). These correlations between marker expression and length of the primary process suggests the existence of a morphological continuum between RGL cells, with proliferation and the expression of stem cell markers decreasing with the shortening of the primary process.

Intriguingly, the frequent production of type  $\beta$  cells upon division of type  $\alpha$  cells does not result in an increase in the number of type  $\beta$  cells over time or in conditions of increased proliferation such as voluntary exercise. This apparent stability in the population of type  $\beta$  cells, together with the absence of microglia engulfment of type  $\beta$  cells also supports the idea of a stable turnover, in which type  $\beta$  cells may transform into astrocytes and migrate out of the GCL. To maintain a stable population of type  $\beta$  cells under conditions of increased or decreased proliferation, the transformation into astrocytes would need to be regulated by the production of type  $\beta$  cells. Time-lapse imaging will shed light in the morphological dynamics and migratory pattern of type  $\beta$  cells.

## CONCLUSION

Together, our results reveal the existence of two morphofunctionally distinct types of RGL cells in the adult dentate gyrus. The selective behavior of these cell types is relevant to the mechanisms of stem cell proliferation and self-renewal. Furthermore, the morphological criteria proposed here may be used to assess the status of the pool of RGL stem cells in the dentate gyrus.

## ACKNOWLEDGMENTS

We thank the Cellular Imaging Facility of the University of Lausanne and Jacqueline Kocher-Braissant for technical help. This work was supported by the Swiss National Science Foundation (to E.G., S.S., F.U., P.-J.G., and N.T.), the Deutsche Forschungsgemeinschaft (Grant DFG LI 858/9-1), and the Bavarian Research Network on Human-induced Pluripotent Stem Cells "ForiPS" (to D.C.L.), the Deutsche Forschungsgemeinschaft (Grant BE5136/1-1) (to R.B.), NIH (Grants

NS048271 and MH105128), Dr. Miriam and Sheldon G. Adelson Medical Research Foundation (to G.-L.M.), and NIH (NS047344; to H.S.). M.A.B. is currently affiliated with the Eli and Broad CIRM Center for regenerative Medicine and Stem Cell Research, University of Southern California, Los Angeles, California, USA.

manuscript; M.A.B., R.B., and S.S.: performed the experiments, discussed the data; F.U. and P.-J.G.: performed the experiments; D.C.L.: discussed the data; G.-L.M.: provided financial support; H.S.: discussed the data, provided financial support; N.T.: conceived and designed the experiments, discussed the data, wrote the manuscript, provided financial support.

#### AUTHOR CONTRIBUTIONS

E.G.: conceived and designed the experiments, performed the experiments, analyzed the data, discussed the data, wrote the

#### POTENTIAL CONFLICTS OF INTEREST

The authors indicate no potential conflicts of interest.

#### REFERENCES

- Altman J, Das GD. Autoradiographic and histological evidence of postnatal hippocampal neurogenesis in rats. *J Compar Neurol* 1965;124:319–335.
- Ming GL, Song H. Adult neurogenesis in the mammalian brain: Significant answers and significant questions. *Neuron* 2011;70:687–702.
- Sahay A, Scobie KN, Hill AS et al. Increasing adult hippocampal neurogenesis is sufficient to improve pattern separation. *Nature* 2011;472:466–470.
- van Praag H, Christie BR, Sejnowski TJ et al. Running enhances neurogenesis, learning, and long-term potentiation in mice. *Proc Natl Acad Sci USA* 1999;96:13427–13431.
- Beckervordersandforth R, Deshpande A, Schaffner I et al. In vivo targeting of adult neural stem cells in the dentate gyrus by a split-cre approach. *Stem Cell Rep* 2014;2:153–162.
- Huttmann K, Sadgrove M, Wallraff A et al. Seizures preferentially stimulate proliferation of radial glia-like astrocytes in the adult dentate gyrus: Functional and immunocytochemical analysis. *Eur J Neurosci* 2003;18:2769–2778.
- Kriegstein A, Alvarez-Buylla A. The glial nature of embryonic and adult neural stem cells. *Ann Rev Neurosci* 2009;32:149–184.
- Mignone JL, Kukekov V, Chiang AS et al. Neural stem and progenitor cells in nestin-GFP transgenic mice. *J Compar Neurol* 2004;469:311–324.
- Steiner B, Klempin F, Wang L et al. Type-2 cells as link between glial and neuronal lineage in adult hippocampal neurogenesis. *Glia* 2006;54:805–814.
- Suh H, Consiglio A, Ray J et al. In vivo fate analysis reveals the multipotent and self-renewal capacities of Sox2 + neural stem cells in the adult hippocampus. *Cell Stem Cell* 2007;1:515–528.
- Lugert S, Basak O, Knuckles P et al. Quiescent and active hippocampal neural stem cells with distinct morphologies respond selectively to physiological and pathological stimuli and aging. *Cell Stem Cell* 2010;6:445–456.
- Noctor SC, Flint AC, Weissman TA et al. Neurons derived from radial glial cells establish radial units in neocortex. *Nature* 2001;409:714–720.
- Shapiro LA, Korn MJ, Shan Z et al. GFAP-expressing radial glia-like cell bodies are involved in a one-to-one relationship with doublecortin-immunolabeled newborn neurons in the adult dentate gyrus. *Brain Res* 2005;1040:81–91.
- Bonaguidi MA, Wheeler MA, Shapiro JS et al. In vivo clonal analysis reveals self-renewing and multipotent adult neural stem cell characteristics. *Cell* 2011;145:1142–1155.
- Gerald J, Sun YZ, Ryan P et al. Tangential migration of neuronal precursors of glutamatergic neurons in the adult mammalian brain. *PNAS* 2015;112:9484–9489.
- Fuentealba MC, Obner K, Alvarez-Buylla A. Adult neural stem cells bridge their niche. *Cell Stem Cell* 2012;10:698–708.
- Shihabuddin LS, Horner PJ, Ray J et al. Adult spinal cord stem cells generate neurons after transplantation in the adult dentate gyrus. *J Neurosci* 2000;20:8727–8735.
- Palmer TD, Willhoite AR, Gage FH. Vascular niche for adult hippocampal neurogenesis. *J Compar Neurol* 2000;425:479–494.
- Lie DC, Colamarino SA, Song HJ et al. Wnt signalling regulates adult hippocampal neurogenesis. *Nature* 2005;437:1370–1375.
- Song H, Stevens CF, Gage FH. Astroglia induce neurogenesis from adult neural stem cells. *Nature* 2002;417:39–44.
- Song J, Zhong C, Bonaguidi MA et al. Neuronal circuitry mechanism regulating adult quiescent neural stem-cell fate decision. *Nature* 2012;489:150–154.
- Gebara E, Sultan S, Kocher-Braissant J et al. Adult hippocampal neurogenesis inversely correlates with microglia in conditions of voluntary running and aging. *Front Neurosci* 2013;7:145.
- Sierra A, Encinas JM, Deudero JJ et al. Microglia shape adult hippocampal neurogenesis through apoptosis-coupled phagocytosis. *Cell Stem Cell* 2010;7:483–495.
- Ashton RS, Conway A, Pangarkar C et al. Astrocytes regulate adult hippocampal neurogenesis through ephrin-B signaling. *Nat Neurosci* 2012;15:1399–1406.
- Nolte C, Matyash M, Pivneva T et al. GFAP promoter-controlled EGFP-expressing transgenic mice: A tool to visualize astrocytes and astrogliosis in living brain tissue. *Glia* 2001;33:72–86.
- Yamaguchi M, Saito H, Suzuki M et al. Visualization of neurogenesis in the central nervous system using nestin promoter-GFP transgenic mice. *Neuroreport* 2000;11:1991–1996.
- Madisen L, Zwingman TA, Sunkin SM et al. A robust and high-throughput Cre reporting and characterization system for the whole mouse brain. *Nat Neurosci* 2010;13:133–140.
- Thuret S, Toni N, Aigner S et al. Hippocampus-dependent learning is associated with adult neurogenesis in MRL/MpJ mice. *Hippocampus* 2009;19:658–669.
- Kuhn HG, Dickinson-Anson H, Gage FH. Neurogenesis in the dentate gyrus of the adult rat: Age-related decrease of neuronal progenitor proliferation. *J Neurosci* 1996;16:2027–2033.
- Sultan S, Gebara EG, Moullec K et al. D-Serine increases adult hippocampal neurogenesis. *Front Neurosci* 2013;7:155.
- Villeda SA, Luo J, Mosher KI et al. The ageing systemic milieu negatively regulates neurogenesis and cognitive function. *Nature* 2011;477:90–94.
- Monje ML, Toda H, Palmer TD. Inflammatory blockade restores adult hippocampal neurogenesis. *Science* 2003;302:1760–1765.
- Encinas JM, Michurina TV, Peunova N et al. Division-coupled astrocytic differentiation and age-related depletion of neural stem cells in the adult hippocampus. *Cell Stem Cell* 2011;8:566–579.
- Filippov V, Kronenberg G, Pivneva T et al. Subpopulation of nestin-expressing progenitor cells in the adult murine hippocampus shows electrophysiological and morphological characteristics of astrocytes. *Mol Cell Neurosci* 2003;23:373–382.
- Sierra A, Martin-Suarez S, Valcarcel-Martin R et al. Neuronal hyperactivity accelerates depletion of neural stem cells and impairs hippocampal neurogenesis. *Cell Stem Cell* 2015;16:488–503.



See [www.StemCells.com](http://www.StemCells.com) for supporting information available online.